PAPER

Check for updates

Al-doping enables high stability of single-crystalline $LiNi_{0.7}Co_{0.1}Mn_{0.2}O_2$ lithium-ion cathodes at high voltage†

Lei Cheng, Bao Zhang, Shi-Lin Su, Lei Ming, [ID]* Yi Zhao and Xin-Xin Tan

$LiNi_{0.7}Co_{0.1}Mn_{0.2}O_2$ (NCM) is a kind of promising cathode material for lithium ion batteries because of its high capacities. However, the further commercialization of this material has been seriously hindered by the unstable structure at a deep de-lithiation state. Herein, it is identified that this drawback can be diminished by Al-doping, which is inherently stable in the lattice framework to restrain the structural collapse of $LiNi_{0.7}Co_{0.1}Mn_{0.2}O_2$ at a high cut-off voltage (4.4 V). As expected, the Al-doped NCM (NCM–0.2Al) material obtains the highest reversible capacity and capacity retention (144.69 mA h g^{-1}, 80.26%) after 90 cycles at 1C. The excellent performance demonstrates that Al-doping can effectively enhance the Li$^+$-ion diffusion kinetic and structural stability of NCM, providing a feasible strategy for the further industrialization of Ni-rich materials.

Introduction

Lithium ion batteries (LIBs), widely used in portable electronic devices and electric vehicles (EVs), have been regarded as the most promising energy storage devices.[1–4] The Ni-rich $LiNi_{1-x-y}Co_xMn_yO_2$ cathode materials have attracted significant attention due to their satisfactory electrochemical properties. However, the application of Ni-rich materials still has many problems, such as cation disordering and structural degradation, which are an intriguing field for the exploration of excellent LIBs.[5–9]

According to the reported articles, the strategy of element doping has been widely used to enhance the reversible capacity of cathode materials at high voltage.[10] Abundant cations doping (Al,[11] W,[12] V,[13] Mg,[14] Zr,[15] Nb[16]) and anion modification (F,[17] N[18]) have been examined by most of researchers all over the world over the past few years. Li *et al.*[11] prepared homogeneously Al-doped NCM811 *via* using a co-precipitation method. The introduction of Al-ion increases the ratio of Ni^{3+} and restrains the cation mixing. Compared with the unmodified samples, the Al^{3+}-doped NCM811 cathode materials showed an excellent cycling and rate performance with a capacity retention of 70% at 10C after 1000 cycles. Shang *et al.*[12] reported a NCM811 cathode material with excellent capability *via* W-doping, its capacity retention of 92.1% at 1C after 100 cycles under 2.8–4.5 V, which could be attributed to the suppression of structure collapse upon cycling and discharge voltage decline by W-doping.

School of Metallurgy and Environment, Central South University, Changsha 410083, P. R. China

However, the homogeneity of the element doping for Ni-rich materials remains a key area to explore for extraordinary cycling stability.[19,20]

Based on the comprehensive consideration of the above reasons, in this work, a simple co-precipitation method has been designed to synthesize Al-doped precursor with small particle size, and subsequently the Al-doped $LiNi_{0.7}Co_{0.1}Mn_{0.2}O_2$ (NCM–0.2Al) single crystal is obtained by using a solid-state method. In addition, the doping in the precursor is beneficial to reduce the energy potential, resulting in more uniform element distribution and less disadvantages of bonding during the later calcination process. Notably, the NCM–0.2Al single crystal cathode material exhibits excellent cycling ability at high cut-off voltage of 4.4 V, owing to the designed geometry of the single crystal and the Al-doping, which can suppress the mixing effect and alleviate the structure collapse of the material during the charging process.

Experimental details

Materials preparation

The typical schematic diagram for preparing the Al-doped $LiNi_{0.7}Co_{0.1}Mn_{0.2}O_2$ materials is illustrated in Fig. 1a. The Al-doped $Ni_{0.7}Co_{0.1}Mn_{0.2}(OH)_2$ precursors were prepared *via* employing a controlled co-precipitation strategy. Typically, an aqueous solution (2 mol L^{-1}) of $NiSO_4 \cdot 6H_2O$, $CoSO_4 \cdot 7H_2O$, $MnSO_4 \cdot H_2O$ with the molar ratio of 7 : 1 : 2 (Ni : Co : Mn), an aqueous solution of AlO_2^- synthesized by mixing the solution of NaOH and $Al_2(SO_4)_3 \cdot 18H_2O$, NaOH solution (4 mol L^{-1}), and $NH_3 \cdot H_2O$ solution (10 mol L^{-1}) were fed into the stainless-steel reactor (50 L) under N_2 atmosphere. Then, the precursors with different Al mass ratios (0%, 0.1%, 0.2% and 0.3%) were obtained
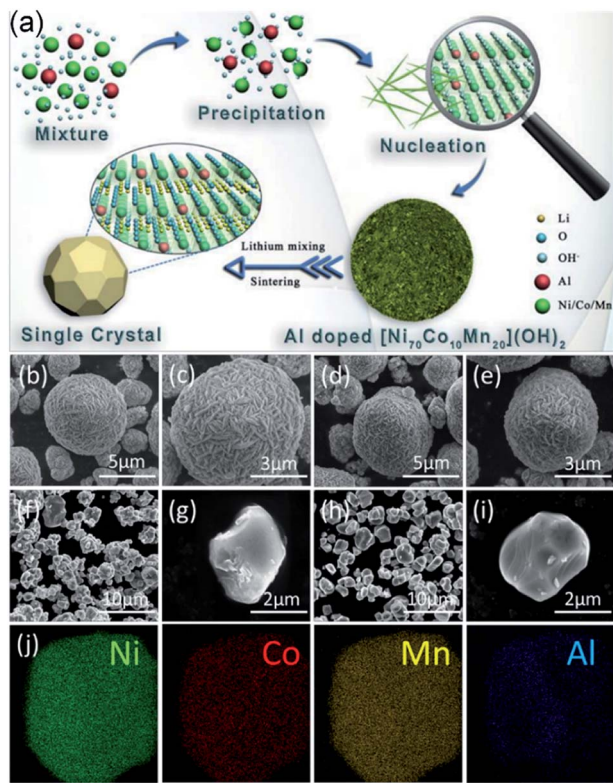
Fig. 1 (a) The illustration of the formation of Al-doped $LiNi_{0.7}Co_{0.1}Mn_{0.2}O_2$ (NCM−0.2Al) materials; the SEM images of (b and c) NCMOH and (d and e) NCMOH−0.2Al, (f and g) NCM and (h and i) NCM−0.2Al, (j) elemental mappings of NCM−0.2Al.

after washing and drying, which were denoted as NCMOH, NCMOH−0.1Al, NCMOH−0.2Al and NCMOH−0.3Al, respectively. The Al-doped $LiNi_{0.7}Co_{0.1}Mn_{0.2}O_2$ materials were prepared by calcining the mixture ($LiOH \cdot H_2O$ and Al-doped precursors, the Li/M molar ratio is 1.05 : 1) at 500 °C for 6 h and 850 °C for 14 h under oxygen atmosphere, which were named as NCM−0.1Al, NCM−0.2Al and NCM−0.3Al. For comparison, the pristine $LiNi_{0.7}Co_{0.1}Mn_{0.2}O_2$ (NCM) could be synthesized by using the same procedure, but without Al-doping.

Materials characterization

The phase composition of the as-prepared products was characterized by X-ray diffraction (XRD, Rigaku, Rint-2000, Cu Kα radiation) with a scanning speed of 10° min^{-1}. Meanwhile, the refined results were calculated with Rietveld method by the GSAS software. The surface chemical valence state of all samples was examined by XPS (Thermo ESCALAB 250XI). The morphology and microstructure were conducted by field-emission scanning electron microscopy (FESEM, JEOL, JSM-6700F) with an energy-dispersive spectrometer (EDS) and a transmission electron microscope (TEM FEI TF20 and JEM-2100F).

Electrochemical evaluation

The electrochemical performance was investigated by CR2032-type coin half-cells. The working electrodes were composed of

80 wt% active materials, 10 wt% acetylene black, and 10 wt% poly(vinylidene difluoride) as binder. NMP (N-methyl-2-pyrrolidone) was used as the solvent. The mixed slurry was coated onto a piece of aluminium foil, dried in a vacuum oven at 80 °C for 12 h, and then cut into discs with a diameter of 13 mm. Lithium foil was used as the reference electrode. $LiPF_6$ (1 M) in ethylene carbonate and diethyl carbonate (EC/DEC, 1 : 1 by volume) was used as the electrolyte. Galvanostatic charge/discharge cycling was conducted between 3.0 V and 4.4 V (vs. Li/Li$^+$, 1C = 170 mA h g^{-1}) at 25 °C with a testing system (LAND CT2001). Electrochemical Impedance Spectroscopy (EIS) tests were recorded with the amplitude voltage of 5 mV in the frequency range of 10 mHz to 100 kHz through an electrochemical workstation (CHI760E). The cyclic voltammetry (CV) was also performed by electrochemical workstation during 3.0–4.4 V.

Results and discussion

The SEM images of precursors are shown in Fig. 1(b–e). All of the precursors display a micro-sized spherical structure with the particle size of ∼4 μm, composed of many nanosheets. The morphologies of NCM and NCM−0.2Al are also characterized by SEM measurements in Fig. 1(f–i). The two samples show the single crystal particles with the grains size of about 2 μm, which are inherited from the spherical precursors with the particle size of around 4 μm. NCM−0.2Al sample has more dispersible
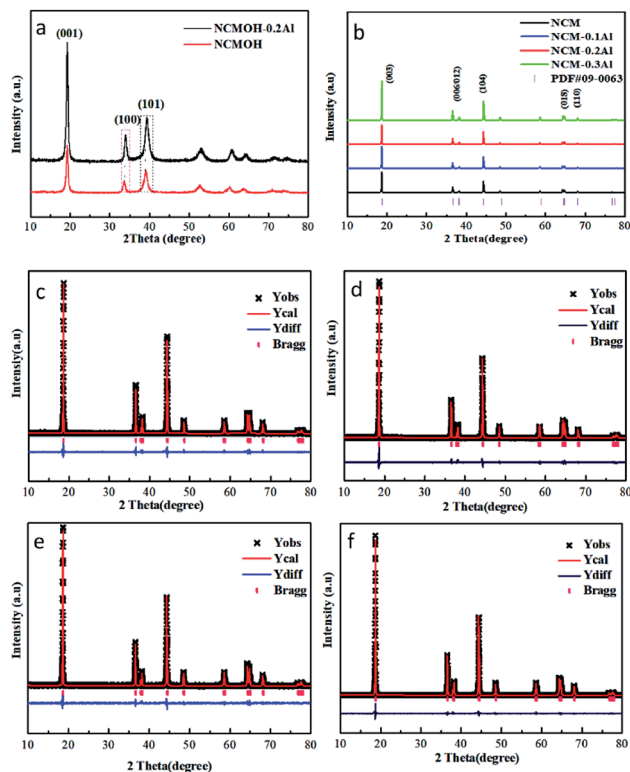

Fig. 2 XRD patterns of (a) NCMOH and NCMOH−0.2Al, (b) NCM and Al-modified cathode materials, Rietveld refinement of (c) NCM, (d) NCM−0.1Al, (e) NCM−0.2Al, (f) NCM−0.3Al.

and exposed surfaces, which can better expose the electrochemical active surface and have a positive effect on the electrochemical properties. All of the elements (including Ni, Co, Mn) are evenly distributed in the bulk of NCM–0.2Al sample (Fig. 1j), and the uniform distribution of Al element in NCM–0.2Al sample confirms that Al ions have been efficiently incorporated into the NCM materials by the calcination process.

Fig. 2a displays the similar XRD results of pristine NCMOH and NCMOH–0.2Al. The peaks of NCMOH–0.2Al shift to the high degree compared with NCMOH, indicating the successful introduction of Al atoms.[21–23] All the spectra of cathode materials (Fig. 2b) are indexed to the α-NaFeO$_2$ phase with $R\bar{3}m$ space group (JCPDS no. 09-0063), which are consistent with the layered structure. The Rietveld refinements results of all the NCM samples are revealed in Fig. 2(c–f) and Table S1.† The low error factors (R_p and R_{sp}) validate the veracity of refinement results. It is indicated that NCM–0.2Al shows the highest value of c/a and the lowest Li$^+$/Ni^{2+} mixing ratio, indicating the well layered structure and excellent Li$^+$ diffusion path of the modified NCM. The contents of Al and other elements have been confirmed by ICP and the results have been displayed in Table S2.†

The crystal structure of NCM and NCM–0.2Al has been investigated by TEM and HRTEM for further, as shown in Fig. 3. The HRTEM image of NCM taken from the selected area in Fig. 3a displays an interplanar distance of 0.245 nm, which matches well with the (101) plane. Meanwhile, the interplanar distance of NCM–0.2Al is also about 0.245 nm (Fig. 3b). These results demonstrate that the Al-doped process hardly changes the crystal structure of the pristine materials.

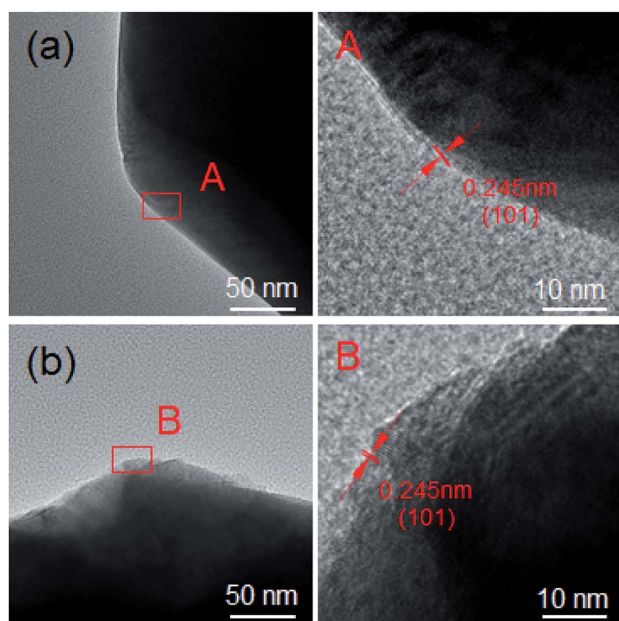In order to further verify the effect of Al-doping, XPS was performed to investigate the chemical states and surface
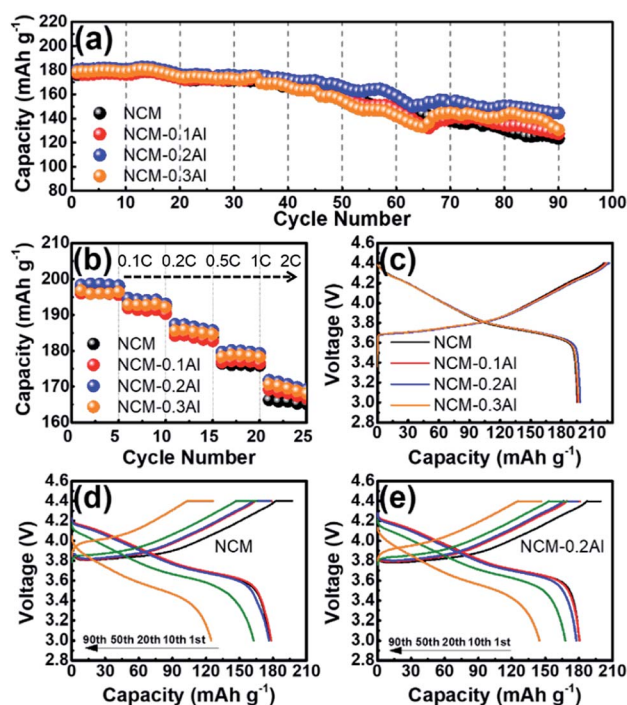

Fig. 4 The cycling performance at 1C (a), rate capacity at various rate from 0.1C to 2C (b) and charge–discharge curves for the 1st cycle at 0.1C (c) of NCM and Al-modified cathode materials; the charge–discharge curves at different cycles at 1C for (d) NCM and (e) NCM–0.2Al.

valence of NCM and NCM–0.2Al. As shown in Fig. S1,† the reduced ratio of Ni^{2+}/Ni^{3+} of NCM–0.2Al is beneficial to diminish the cation mixing and stabilize the structure of the materials. Meanwhile, the reduced oxygen defects of NCM–0.2Al materials effectively enhanced the structural stability.[23] The similar Co 2p and Mn 2p spectra for NCM and NCM–0.2Al indicate that there is no valence change of Co and Mn element after Al-doping.

To verify the impact of Al-doping for strengthening the structure stability, the long cycling performance of all the samples was performed between 3.0 V and 4.4 V at 25 °C (Fig. 4a). At a current density of 1C, the capacity retention of NCM–0.2Al is above 80% after 90 cycles, which is higher than that of NCM (about 70%). Meanwhile, the sample of NCM–0.2Al delivers the best rate capability than others, especially at high rate (Fig. 4b). The initial charge/discharge curves of NCM and Al-doped NCM at 0.1C are presented in Fig. 4c. The similar profiles of all samples indicate that the doped process has no negative effect on the lithium-ion insertion/extraction behaviours. Comparing the charge/discharge curves of NCM and NCM–0.2Al cathode materials (Fig. 4d and e), the sample of NCM–0.2Al delivers better cycling stability than that of pristine material.

To further demonstrate the different electrochemical behaviours of NCM and NCM–0.2Al, the differential capacity profiles have been employed in Fig. 5a and b. The oxidation peaks (around 3.82 V) of NCM–0.2Al at first cycle shift slightly toward a lower potential compared with that of the pristine
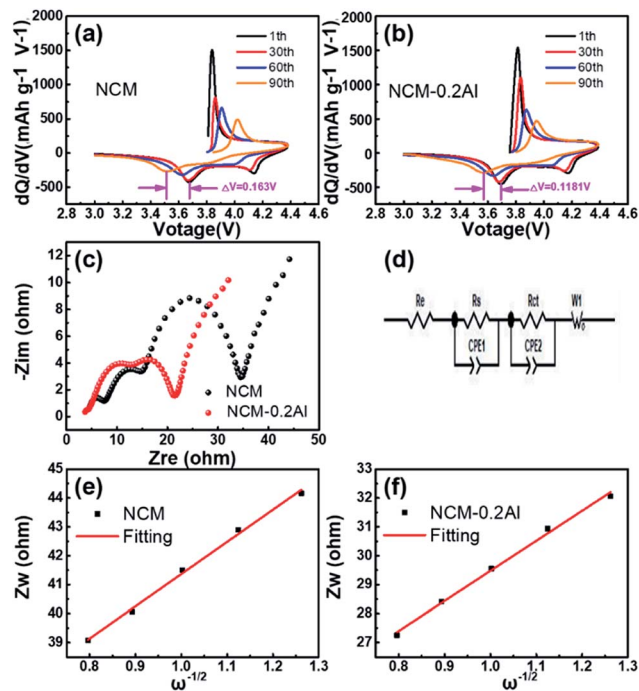

Fig. 3 The TEM and corresponding HRTEM images of (a) NCM and (b) NCM–0.2Al.

Fig. 5 (a and b) dQ/dV curves during long cycling of NCM and NCM–0.2Al, (c) Nyquist curves of NCM and NCM–0.2Al, (d) equivalent circuit model used for fitting the experimental EIS data, (e and f) the plots of Z_w–$\omega^{-1/2}$.

(3.94 V), indicating the reduced Ni^{2+} contents and alleviative polarization of NCM–0.2Al materials by the strategy of Al-doping.[24–26] In addition, the EIS results after 90 cycles (Fig. 5c, d and Table S3†) illustrate that the sample of NCM–0.2Al possesses the lower resistance value and higher D_{Li^+} (5.3278 × 10^{-11} cm² s⁻¹) than that of NCM (4.6542 × 10^{-11} cm² s⁻¹), showing the superior reaction kinetics.[7,27–31]

Meanwhile, the outstanding cycling stability of NCM–0.2Al also has been confirmed by the cross-sectional SEM images
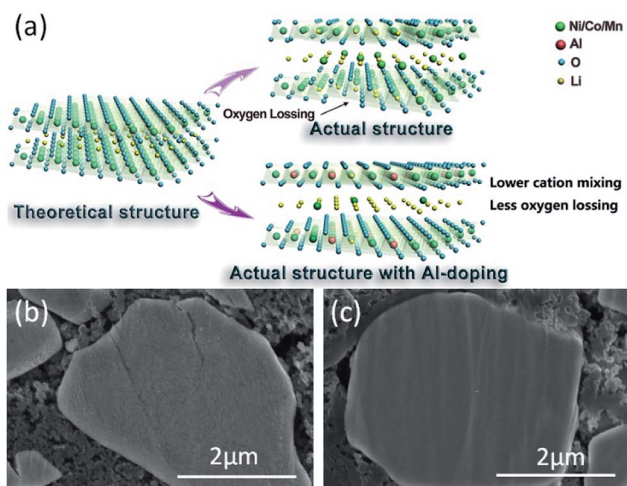

Fig. 6 (a) Schematic illustration of structure for the Al-doping NCM; SEM images of the cross-sections of the (b) NCM and (c) NCM–0.2Al cathodes after 90 cycles at 25 °C.

(Fig. 6b and c), which delivers unbroken crystal framework. Based on the above results, the excellent properties of NCM–0.2Al are mainly attributed to the stable structure enabled by Al-doping and the vivid scheme has been illustrated in Fig. 6a.

Conclusions

In summary, the Al-doped $LiNi_{0.7}Co_{0.1}Mn_{0.2}O_2$ (NCM–0.2Al) single crystal materials with excellent Li^+-ion storage properties were obtained by the co-precipitation and post-calcination method. The excellent electrochemical performance of NCM–0.2Al can be attributed to the stable structure enabled by Al-doping, which can effectively restrain volume change during cycling and alleviate the mixing of Ni^{2+}/Li^+. In addition, NCM–0.2Al sample owns a small charge transfer impedance and large Li^+-ion diffusion kinetic, which is beneficial to improve the rate performance of the electrode material.

Conflicts of interest

There are no conflicts to declare.

Acknowledgements

Notes and references

1 T. Chen, X. Li, H. Wang, X. Yan, L. Wang, B. Deng, W. Ge and M. Qu, J. Power Sources, 2018, 374, 1–11.

2 Z. Zhao, S. Chen, D. Mu, R. Ma, C. Li, B. Wu, F. Wu, K. Cheng and C. Xie, J. Power Sources, 2019, 431, 84–92.

3 D. Zuo, G. Tian, X. Li, D. Chen and K. Shu, J. Alloys Compd., 2017, 706, 24–40.

4 F. Zheng, X. Ou, Q. Pan, X. Xiong, C. Yang and M. Liu, J. Power Sources, 2017, 346, 31–39.

5 K. Yuan, N. Li, R. Ning, C. Shen, N. Hu, M. Bai, K. Zhang, Z. Tian, L. Shao, Z. Hu, X. Xu, T. Yu and K. Xie, Nano Energy, 2020, 78, 105239.

6 K. Marker, C. Xu and C. P. Grey, J. Am. Chem. Soc., 2020, 142, 17447–17456.

7 J. Zhang, J. Zhang, X. Ou, C. Wang, C. Peng and B. Zhang, ACS Appl. Mater. Interfaces, 2019, 11, 15507–15516.

8 Q. Q. Qiu, Z. Shadike, Q. C. Wang, X. Y. Yue, X. L. Li, S. S. Yuan, F. Fang, X. J. Wu, A. Hunt, I. Waluyo, S. M. Bak, X. Q. Yang and Y. N. Zhou, ACS Appl. Mater. Interfaces, 2019, 11, 23213–23221.

9 Y. Shi, G. Chen, F. Liu, X. Yue and Z. Chen, ACS Energy Lett., 2018, 3, 1683–1692.

10 X. Zeng, J. Zhu, L. Yang, L. Zhou, L. Shao, S. Hu, C. Huang, C. Yang, D. Qian and X. Xi, J. Electroanal. Chem., 2019, 838, 94–100.

11 Y.-C. Li, W. Xiang, Z.-G. Wu, C.-L. Xu, Y.-D. Xu, Y. Xiao, Z.-G. Yang, C.-J. Wu, G.-P. Lv and X.-D. Guo, Electrochim. Acta, 2018, 291, 84–940.

12 G. Shang, Y. Tang, Y. Lai, J. Wu, X. Yang, H. Li, C. Peng, J. Zheng and Z. Zhang, *J. Power Sources*, 2019, **423**, 246–254.

13 S.-J. Sim, S.-H. Lee, B.-S. Jin and H.-S. Kim, *Sci. Rep.*, 2019, **9**, 8952.

14 S. S. Zhang, *Energy Storage Mater.*, 2020, **24**, 247–254.

15 C. S. Yoon, M.-J. Choi, D.-W. Jun, Q. Zhang, P. Kaghazchi, K.-H. Kim and Y.-K. Sun, *Chem. Mater.*, 2018, **30**, 1808–1814.

16 S. Liua, X. Chenb, J. Zhaoa, J. Sub, C. Zhangb, T. Huangb, J. Wuc and b. Aishui Yua, *J. Power Sources*, 2018, **374**, 149–157.

17 P. Yue, Z. Wang, H. Guo, X. Xiong and X. Li, *Electrochim. Acta*, 2013, **92**, 1–8.

18 J. O. Binder, S. P. Culver, R. Pinedo, D. A. Weber, M. S. Friedrich, K. I. Gries, K. Volz, W. G. Zeier and J. Janek, *ACS Appl. Mater. Interfaces*, 2018, **10**, 44452–44462.

19 X. X. Dong, C. Y. Huang, Q. Jin, J. Zhou, P. Feng, F. Y. Shi and D. Y. Zhang, *RSC Adv.*, 2017, **7**, 33745–33750.

20 L. Ming, B. Zhang, C. Wang, X. Ou, J. Zhang and Z. Yang, *Chem. Phys. Lett.*, 2020, **741**, 137090.

21 Y. Mo, L. Guo, B. Cao, Y. Wang, L. Zhang, X. Jia and Y. Chen, *Energy Storage Mater.*, 2019, **18**, 260–268.

22 U.-H. Kim, S.-T. Myung, C. S. Yoon and Y.-K. Sun, *ACS Energy Lett.*, 2017, **2**, 1848–1854.

23 B. Zhang, L. Wang, Y. Zhang, Y. Ding and Y. Bi, *Angew. Chem., Int. Ed.*, 2018, **57**, 2248–2252.

24 X. Xu, H. Huo, J. Jian, L. Wang, H. Zhu, S. Xu, X. He, G. Yin, C. Du and X. Sun, *Adv. Energy Mater.*, 2019, **9**, 1803936.

25 Y. Han, S. Heng, Y. Wang, Q. Qu and H. Zheng, *ACS Energy Lett.*, 2020, **5**, 2421–2433.

26 C. S. Yoon, D.-W. Jun, S.-T. Myung and Y.-K. Sun, *ACS Energy Lett.*, 2017, **2**, 1150–1155.

27 X. Wang, H. Wang, M. Liu and W. Li, *Small*, 2020, **16**, e2000769.

28 C. Wang, L. Shao, X. Guo, X. Xi, L. Yang, C. Huang, C. Zhou, H. Zhao, D. Yin and Z. Wang, *ACS Appl. Mater. Interfaces*, 2019, **11**, 44036–44045.

29 C. Wang, B. Zhang, H. Xia, L. Cao, B. Luo, X. Fan, J. Zhang and X. Ou, *Small*, 2020, **16**, e1905853.

30 M. H. Alfaruqi, S. Islam, J. Song, S. Kim, D. T. Pham, J. Jo, S. Kim, J. P. Baboo, D. Y. Putro, V. Mathew and J. Kim, *Chem. Phys. Lett.*, 2017, **681**, 44–49.

31 C. Wang, C. Zhou, B. Zhang, X. Ou, L. Cao, C. Peng and J. Zhang, *RSC Adv.*, 2019, **9**, 9075–9078.